Available online at www.sciencedirect.com
ScienceDirect
International Journal of Heat and Mass Transfer 50 (2007) 1469–1484
International Journal of HEAT and MASS TRANSFER
www.elsevier.com/locate/ijhmt

Thermal dispersion for water or air flow through a bed of glass beads

A. Testu [a,c], S. Didierjean [a], D. Maillet [a,*], C. Moyne [a], T. Metzger [b], T. Niass [c]

[a] LEMTA, UMR, Universite Henri Poincare, Institut National Polytechnique de Lorraine, 2 Avenue de la Forêt de Haye, 54504 Vandoeuvre les Nancy, France
[b] Fakultät für Verfahrens- und Systemtechnik, Otto-von-Guericke-Universität, Universitätsplatz 2, 39106 Magdeburg, Germany
[c] Institut Français du Pétrole, CEDI, René Navarre, BP no. 3, 69390 Vernaison, France

Received 28 February 2006; received in revised form 6 September 2006
Available online 7 November 2006

Abstract

The one-temperature model for thermal dispersion in a porous medium is based on the notion of an average 'enthalpic' temperature, solution of an energy equation of the convection–diffusion type. It requires the determination of thermal dispersion coefficients. The functional form of the correlations that relate them to dimensionless groups is established as well as the limits of this model. An experimental bench has been built to measure these coefficients for water or air flow through a bed of glass beads. They are estimated through a Bayesian inversion of several local temperature measurements, with uncertainty on their location, and with the use of the analytical solution of a corresponding model. Results are presented in terms of variation of these two coefficients with the Reynolds or Péclet numbers and with the nature of the fluid and corresponding correlations are given.

Keywords: Thermal dispersion coefficients; Correlation; One-temperature model; Local temperature equilibrium

1. Introduction

Thermal dispersion in a porous medium results from the combined effects of heat diffusion in both the fluid and solid phases and thermal convection in the fluid. We consider here a homogeneous porous medium only, that is a porous medium whose constituents and microscopic (local) structure do not depend on the region that is considered. In the absence of convection in such a medium, conduction can be characterized, at the mesoscopic scale, by a single equivalent or effective conductivity if the medium is isotropic at the local scale: a thermal disturbance diffuses the same way in all the directions. This single parameter depends on the thermophysical properties of the components, on the porosity of the medium, on the nature and the geometry of the grains, etc. Things change when the fluid phase starts to move under the effect of an external cause (gravity, pump, fan, etc.): one observes that heat is transferred mainly in the direction of the average flow. Simple addition of a convective term in the energy equation (of the equivalent homogenized medium) does not allow to take into account the hydrodynamic effects properly. It is necessary to add dispersion terms that are not based on an isotropic conductivity but rather on a non spherical dispersion tensor whose coefficients depend in particular on the local Darcy or filtration velocity of the flow.

Modelling and simulation of simultaneous conduction and convection at the scale of the pores requires the solution of the local heat equations written for the two phases (fluid and solid) and on the Navier–Stokes equations in the fluid. The difficulties related to the solution of these equations are very large: they are not only numerical but also stem from the absence of precise knowledge of the local structure of the material. A more practical approach consists in seeking a characterization of the medium at the mesoscopic scale that results from some kind of averaging of the variables of the local model (velocity and temperature fields). In order to derive such a reduced model for

* Corresponding author. Tel.: +33 03 83 59 56 06; fax: +33 03 83 59 55 31.
E-mail address: denis.maillet@ensem.inpl-nancy.fr (D. Maillet).

0017-9310/$ - see front matter © 2006 Elsevier Ltd. All rights reserved.
doi:10.1016/j.ijheatmasstransfer.2006.09.002

Nomenclature

a	thermal diffusivity ($m^2 s^{-1}$)
a_{sf}	specific area (m^{-1})
b	bias
c_p	heat capacity ($J K^{-1} kg^{-1}$)
d, D	particle diameter and diameter of the averaging sphere (m)
e, f, k, m	Green's functions
h, h_∞	impedance ($J m^{-2} K$), or heat exchange coefficient ($W m^{-2} K$)
g, $\boldsymbol{k}$, ℓ	functions
H	volumetric enthalpy ($J m^{-3}$) or Heaviside function
L	macroscopic length (m)
$\boldsymbol{n}$	normal unit vector
p	Laplace parameter (m^{-1})
$\hat{p}$	driving pressure (Pa)
Pe	particulate Péclet number ($u_D d/a_f$)
Pr	Prandtl number ($c_p\mu/\lambda$)
q	normalized square root of the Laplace parameter
$q_{s\to f}$	volumetric heat power exchanged between solid and fluid phases ($W m^{-3}$)
Q	lineic heating power ($W m^{-1}$)
$\boldsymbol{r}$, $\boldsymbol{r}'$	position vector
R	particle radius ($=d/2$) (m)
$Re = Re_d$	particulate Reynolds number ($u_D d/v_f$)
s	volumetric heat source ($W m^{-3}$), or statistical standard deviation
S	least squares sum
t	time (s)
T	temperature (K)
T_H	enthalpic mean temperature (K)
$\boldsymbol{u}_D$, u	Darcy (or superficial or filtration) velocity ($m s^{-1}$)
u^*	corrected Darcy velocity, $(\rho c_p)_f u/(\rho c_p)_t$
v	local velocity ($m s^{-1}$)
V	volume of the representative averaging sphere (m)
x, y, z	space coordinates (m)
X_j	sensitivity coefficient of temperature to parameter βj

Greek symbols

α, β	vector of parameters
δ	Dirac distribution (s^{-1}) or (m^{-1})
ε	volumetric fraction or porosity
λ	thermal conductivity ($W m^{-1} K^{-1}$)
λ_{eq}	equivalent thermal conductivity ($W m^{-1} K^{-1}$)
λ, λ_x, λ_y	thermal dispersion tensor and its coefficients ($W m^{-1} K^{-1}$)
Λ_f	dispersivity tensor of the fluid phase ($W m^{-1} K^{-1}$)
μ	dynamics viscosity ($kg m^{-1} s^{-1}$)
v_f	kinematic viscosity ($m^2 s^{-1}$)
ρ	density ($kg m^{-3}$)
σ	stochastic standard deviation

Subscripts

eq	equivalent property of the homogenized porous medium
exp	experimental value
f	fluid phase
s	solid phase
t	total, relative to both solid and fluid phases
ref	relative to a reference temperature
loc	relative to a local source or to a local Green's function
ave	relative to an averaged source or to an averaged Green's function

Superscripts

~	Laplace transform
*	normalized quantity using the microscopic scale d
°	normalized quantity using a mesoscopic scale D
_	statistical average
^, est	estimated value

heat transfer, techniques such as volume averaging of the local equations can be implemented. This kind of technique leads to various models such as the one-temperature model or the two-temperature model. The parameters of these models are the mean velocity of the flow and the thermal dispersion tensor.

Yagi et al. [1] were the first to measure the effective axial (or longitudinal, that is in the direction of the flow) thermal 'conductivities' of packed beds. Their axial steady state temperature measurements were made using adiabatic double wall evacuated glass pipes. The packed bed was heated from the top by an infra-red lamp so heat penetrated downwards into the bed, while air flowed counter currently upwards through the bed from the bottom inlet. The authors used a linear model to determine the longitudinal thermal dispersion coefficient.

Votruba et al. [2] evaluated the effective axial thermal 'conductivity' from axial temperature distributions for different particle sizes. Measurements of the coefficients were performed using a glass reactor similar to Yagi et al. [1]. Their results were summarized by a correlation giving the effective axial Péclet number as a function of the fluid Péclet number. The coefficients of this correlation depend on the size, shape and nature of the solid particles. Dixon and Cresswell [3] derived a correlation between the effective axial Péclet number and the particulate Péclet number.

Gunn and De Souza [4] made measurements in transient state. They carried out a periodic excitation at the entry of the granular medium and measured the outlet response. They used the two-temperature model for air flow through a dispersed solid phase (glass beads). Because of a low sensitivity of the temperature signal to the model parameters, their results were mainly qualitative and only tendencies could be evidenced.

Tsotsas [5] examined the existing types of models for longitudinal thermal dispersion. Using a momentum analysis, he set up equivalence criteria between these models and derived the velocity dependence of the longitudinal thermal dispersion coefficient.

Concerning lateral or transverse thermal dispersion, that is in the direction normal to the flow, Bauer and Schlünder [6] generalised a heat transport model that is considered as a reference. This model is widely used in the chemical engineering community. It derives from an analogous mass dispersion model based on the assumption of a cascade of perfectly mixed elementary reactors. Levec and Carbonell [7] determined the transverse dispersion coefficient in the stationary case and for local thermal equilibrium. Their method is based on a two-phase model different from the one temperature model presented in Section 2, in which extra terms appear representing a coupling between solid and fluid temperatures, see Zanotti and Carbonell [8]. One should note here that many authors evaluated the lateral dispersion experimentally with experiments where the heating source was located at the bed wall and temperature measured in the core of the bed. In that type of configuration the use of a simple dispersion model could be biased because the near-wall region, where channeling effects take place, cannot be homogenized, see Martin [9].

Metzger et al. [10] estimated the two dispersion coefficients for a packed bed of glass spheres through which water flows. The one-temperature model based on the notion of average enthalpic temperature as detailed in Moyne et al. [11], see Section 2 below, was used. Thermocouples in the downstream neighbourhood of a line heat source, corresponding probably to minimum channelling effects, measured the temperature response to a step heat input. Correlations were proposed to express the dispersion coefficients, even if the lateral dispersion coefficient was not estimated with a high enough precision for sensitivity reasons.

The different correlations for the thermal dispersion coefficients in the literature relate the dispersion coefficient to either the Reynolds or Péclet number. They were often constructed using a single fluid flowing through a given bed.

In order to separate the effect of the Reynolds and Péclet numbers, and to study the effect of the thermal properties of the fluid, it is interesting to make experiments with different fluids in the same solid matrix. When a liquid flows at a very low flow rate through a porous media, it is governed by Darcy's law. Several numerical [12] and experimental results [13,14] have shown that this law is valid only in a narrow range of flow rates. In fact, when the flow rate increases, the pressure drop does not remain proportional to the filtration velocity. The dimensionless number usually used to characterize the onset of this non-linear behaviour is the Reynolds Number (Re) defined with the superficial velocity and a characteristic local scale, which is the sphere diameter for a bed of beads. It is generally admitted that the onset of the non-Darcy flows occurs for Re larger than 10. At high Reynolds number, the empirical Forcheimer equation [15] is used. The use of the Reynolds number is justified for explaining the variation of the thermal dispersion coefficients with fluid velocity when different flow regimes occur.

In this work a pertinent form is looked first for the correlation explaining the variation of the dispersion coefficients (longitudinal and transverse) with the thermophysical characteristics and structure of the porous matrix and with the fluid flow. A particular configuration, that will be used later for estimating the thermal dispersion coefficients, is considered then. The end of this article is devoted to the experimental estimation of both thermal dispersion coefficients in a packed bed of glass beads with the same method as Metzger et al. [10] but with a different fluid, air, and to a comparison of the results for the two fluids (air and water) once suitable correlations have been constructed.

2. One-temperature model

The simplest homogeneous model that can be used to describe thermal dispersion in a granular medium is based on a local mean 'enthalpic' temperature T_H defined at a point P (and for a given time t) in the homogenized medium. This temperature is the space average of the local temperatures at the points P' of the porous medium (P' belonging either to the solid or fluid phase) located inside a sphere of volume $V(P,D)$ of diameter D and centred at P. This sphere should constitute a representative volume of the porous medium. This mean temperature is a weighted average, the local heat capacities $\rho c_p(P')$ being used as weights [11]:

$$T_H(P) = \frac{1}{(\rho c_p)_t V(P,D)} \int_{V(P,D)} \rho c_p(P') T(P') \mathrm{d}V(P') = \frac{1}{(\rho c_p)_t} \langle H \rangle (P) \tag{1}$$

where the total local volumetric heat is:

$$(\rho c_p)_t(P) = \langle \rho c_p \rangle (P) = \varepsilon_f (\rho c_p)_f + \varepsilon_s (\rho c_p)_s, \tag{2a}$$

where ε_f and ε_s are the local volume fractions of the fluid (f) and solid (s) phases and $(\rho c_p)_f$ and $(\rho c_p)_s$ the corresponding volumetric heat capacities. In the preceding equations, $H(P)$ is the local enthalpy by unit volume, $H(P) = \rho c_p(P) T(P)$, and $\langle\,\rangle$ is the averaging operator, defined for any space field f by:

$$\langle f\rangle(P) = \frac{1}{V(P,D)} \int_{V(P,D)} f(P')\mathrm{d}V(P'). \tag{2b}$$

In the preceding equations time t has not been written as an argument of the different functions, in order to simplify the notation. Eq. (1) can be viewed as a filtering, in the data processing meaning, of the local temperature field, the filter used being a moving average of width D. For this homogenisation to be pertinent, the diameter D of the sphere must be much larger than the local characteristic size of the porous medium, here the average diameter d of the grains, and much smaller than the characteristic size L of the system that is modelled, the diameter of the fixed bed reactor for a process engineering application for example.

The local mean temperature T_H used here derives directly from the enthalpic volume average $\langle H\rangle$, which means that it has an energetic meaning. As a consequence, no a priori assumption of local thermal equilibrium is made in its definition and in the use of the reduced one-temperature model that will be presented next. This reduced model requires the definition of a thermal dispersion tensor λ whose coefficients can be considered as pseudo-conductivities depending on the nature, thermophysical properties and geometry of the solid grains and of the fluid, as well as on the local Darcy's (or filtration) velocity $\boldsymbol{u}_D$. A convection–diffusion equation for the space and time variation of the averaged temperature can be written:

$$(\rho c_p)_\mathrm{t} \frac{\partial T_H}{\partial t} = \nabla\cdot(\lambda\nabla T_H) - (\rho c_p)_\mathrm{f} \boldsymbol{u}_D\cdot\nabla T_H + s \tag{3}$$

with:

$$\boldsymbol{u}_D(P) = \langle v\rangle \tag{4}$$

where v is the local fluid velocity, which is equal to zero in the solid phase.

In this equation s is the volumetric heat rate of a source that can depend on both time and space. One can notice that the coefficient of the transient term is the total volumetric capacity $(\rho c_p)_\mathrm{t}$ while the advection term only uses its fluid component $(\rho c_p)_\mathrm{f}$. The preceding Eq. (3) can be derived using either the volume averaging technique or the homogenisation method for a spatially periodic porous medium.

3. Experimental device and corresponding model

One of the methods for testing the validity of a model is to build an experiment designed for estimating (in the statistical sense) the parameters present in this model using measured output (here temperature measurements) for a given (known) input (here some kind of thermal excitation, that is a particular s function in Eq. (3)). Once these parameters estimated, it is possible to reconstruct the theoretical output of the model (the theoretical thermograms here) and to compare it to the experiment output (the experimental thermograms). A final step in the validation of the model consists in comparing the theoretical output of the model (with the previously estimated parameters) with their experimental counterparts for different media, inputs and/or measurement locations. That is this kind of methodology based on the implementation of an inverse experimental technique that has been implemented in the experimental part of this work. The chosen experimental configuration as well as the corresponding model is precised below.

A bed of monodisperse glass beads of diameter $d = 2$ mm has been constructed by filling a box with the beads. Its porosity was $\varepsilon = \varepsilon_\mathrm{f} = 0.365$. The heat source was an electrically heated wire defining the z-direction and set normally to the x–y plane and at the origin ($x = y = 0$) of the coordinate system shown in Fig. 1.

The fluid flowed vertically downwards in the x-direction normal to the wire, with a uniform filtration velocity $u = u_{Dx}$ in the x-direction, through the granular medium. Starting from thermal equilibrium at temperature T_0, that is for equal temperatures for both the incoming fluid and the uniform temperature bed, the wire was submitted to a power step of lineic power intensity $Q(\mathrm{W\,m^{-1}})$ at time $t = 0$. The medium was large enough to be considered as infinite, which means that the one-temperature model temperature response to this excitation is $\Delta T = T_H - T_0$ and is equal to zero at large distances from the source. Renaming T the ΔT response and assuming that the principal directions of the dispersion tensor are the longitudinal (x) and transverse (y) directions, Eq. (3) becomes:

$$(\rho c_p)_\mathrm{t} \frac{\partial T}{\partial t} = \lambda_x \frac{\partial^2 T}{\partial x^2} + \lambda_y \frac{\partial^2 T}{\partial y^2} - (\rho c_p)_\mathrm{f} u \frac{\partial T}{\partial x} + Q\delta(x)\delta(y)H(t) \tag{5}$$

where $\delta(\cdot)$ is the Dirac distribution and $H(\cdot)$ the Heaviside function. In order to prevent any non-linear effect caused by variation with temperature of the different thermophysical properties of both fluid and grains – mass density,

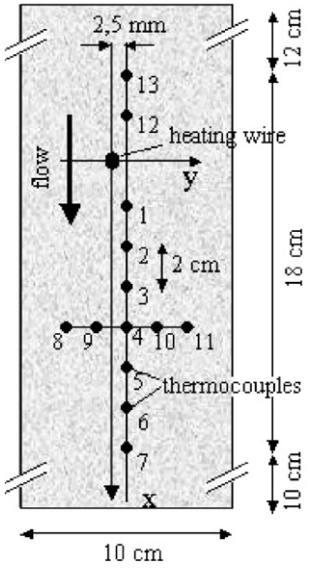

Fig. 1. Dimensions of the granular media and positions of thermocouples.

Table 1
Thermal properties at 20 °C of the two phases of the granular bed. The last two columns gives the corresponding properties of the homogenized equivalent systems ($(\rho c_p)_t$, λ_{eq},ε)

	Water	Air	Glass	Water/glass	Air/glass
(ρc_p) (kJ/m^3)	4170	1.2	2080	2840	1320
λ (W/m/K)	0.607	0.026	1	0.860	0.2
ε				0.365	0.365
ν_f (m^2/s)	0.101×10^{-5}	1.57×10^{-5}			
Pr	7.02	0.7			

viscosity, thermal conductivities – the level of the heat step Q was chosen low enough to get a temperature rise lower than one Celsius degree. This assumption of constant dispersion coefficients λ_x and λ_y, volumetric heat capacities and filtration velocity makes Eq. (5) linear. This equation can be solved using the Green's function technique [16]:

$$T(x,y,t) = \frac{Q}{4\pi\sqrt{\lambda_x\lambda_y}} \exp\left(\frac{(\rho c_p)_f u x}{2\lambda_x}\right) \times \int_0^{\frac{(\rho c_p)_f^2 u^2 t}{4(\rho c_p)_t \lambda_x}} \exp\left(-\left(\frac{x^2}{\lambda_x}+\frac{y^2}{\lambda_y}\right)\frac{(\rho c_p)_f^2 u^2}{16\lambda_x}\frac{1}{\theta}-\theta\right)\frac{d\theta}{\theta}. \quad (6)$$

Either water or air could flow downwards through the stacked bed shown in Fig. 1. The initial bench [10,19] that used a water flow produced by a pump fed by a closed-loop constant hydraulic head circuit, has been modified for an air flow: a fan located in a cylindrical duct downstream the setup aspired air from a high volume room upstream through a second upstream cylindrical duct. The large volume of the upstream room allowed a quasi-constant temperature for the air input.

Thirteen thermocouples, of type *E* and of 127 μm diameter, set parallel to the wire and located mainly downstream the heating wire, measured the temperature response of the medium to the power step. The air velocity could be measured by a hot wire anemometer in the downstream cylindrical duct. The thermal properties of both phases and the equivalent properties of the homogenized medium studied in this article are given in Table 1.

Measurements have been made for particulate Péclet numbers *Pe* from 10 to 70 in the case of air flow, which corresponds to maximum filtration velocities close to 0.7 m/s. For water flow the Péclet number varied between 10 and 130, with maximum filtration velocities of the order of 7 mm/s.

4. Pertinent correlations for the thermal dispersion coefficients

The dispersion coefficients of the one-temperature model, Eqs. (1)–(4), result from an up-scaling process. Their values derive from a closure problem whose solution can be found numerically only if the medium and its internal flow are perfectly known. This knowledge must concern its structure, that is the location of the fluid/solid interface, the thermophysical properties of the two phases as well as the structure of the velocity field at the local scale. For a very limited number of academic cases an analytical expression can be found. Such is the case for λ_x in a periodic porous medium where the unit cell corresponds to a fully developed flow between two parallel plates where Taylor's dispersion occurs [11]. The internal structure of real porous media is generally unknown at the local scale, which makes the attempts of solution of the previous closure problem quite academic. It is another path that will be followed here, that is the construction of heat transfer correlations. These correlations will not deal with a h coefficient, as in external boundary layer flow or in internal duct flow, that is not pertinent in this kind of situation, but with the dispersion coefficients themselves. In order to define the non dimensional parameters that explain the variation of these coefficients both the equations of the local coupled conduction–convection problem and of the corresponding one-temperature model will be derived first. In a second stage these equations will be written in a dimensionless form using suitable scales for all the quantities, in order to make the structure of the desired correlations naturally appear.

We consider the flow of a fluid in a porous medium, at the local scale: all the thermophysical properties of both fluid and solid phases are assumed to be constant. The transfer and transport equations in the parts of the total infinite volume Ω, occupied by the fluid (Ω_f) or by the solid (Ω_s) phases, are:

$$\nabla\cdot v = 0; \quad \frac{dv}{dt} = \frac{\partial v}{\partial t} + v\cdot\nabla v = -\frac{1}{\rho_f}\nabla\hat{p} + \nu_f\nabla^2 v \quad \text{in} \quad \Omega_f \quad (7a)$$

$$(\rho c_p)_f \frac{dT_f}{dt} = (\rho c_p)_f\left(\frac{\partial T_f}{\partial t} + v\cdot\nabla T_f\right) = \lambda_f\nabla\cdot\nabla T_f + s_f \quad \text{in} \quad \Omega_f \quad (7b)$$

$$(\rho c_p)_s \frac{\partial T_s}{\partial t} = \lambda_s\nabla\cdot\nabla T_s + s_s \quad \text{in} \quad \Omega_s \quad (7c)$$

where v is the local velocity vector, $\hat{p} = p + \rho g z$ the modified pressure where z is the height of the corresponding point, g the gravity and p the pressure, ρ_f and ν_f the density and kinematics viscosity of the fluid, λ_f and λ_s the fluid and solid conductivities and s_f and s_s the volumetric heat sources in both phases. The accompanying interface, boundary and initial conditions are:

$$T_s = T_f \quad \text{and} \quad -\lambda_s\nabla T_s\cdot\boldsymbol{n}_s = -\lambda_f\nabla T_f\cdot\boldsymbol{n}_s \quad \text{on } \partial\Omega_{sf}, \quad (7d)$$

$$T_s - T_f \to 0 \quad \text{and} \quad T_s \to T_{ref} \quad \text{as } \|r\| \to \infty, \quad (7e)$$

$$T_s = T_f = T_{ref} \quad \text{at } t = 0 \text{ in } \Omega = \Omega_f U \Omega_s, \quad (7f)$$

where $\boldsymbol{r} = \boldsymbol{OP}$ is the position vector of a point P, $\boldsymbol{n}_s$ the local normal unit vector at the solid–fluid interface $\partial\Omega_{sf}$.

T_{ref} is a reference temperature that is equal to the initial (uniform) temperature and to the temperature at the boundaries of the infinite medium. In order to completely close the problem, it is necessary to add some initial and boundary (or periodicity) conditions that involve pressure and/or velocity for the fluid flow problem.

Reduction of the following equations can be made using a local length scale, here an average pore or grain diameter d, a reference average velocity v_∞, and a reference temperature difference $\Delta T_{\text{ref}} = T_0 - T_{\text{ref}}$. The new dimensionless quantities are then:

$$\begin{aligned} &\boldsymbol{r}^* = \boldsymbol{r}/d; \quad v^* = v/v_\infty; \quad t^* = v_\infty t/d; \quad \hat{p}^* = \hat{p}/\rho_{\text{f}} v_\infty^2; \\ &T^* = (T - T_{\text{ref}})/\Delta T_{\text{ref}}; \quad s^*_{\text{s or f}} = d s_{\text{s or f}}/[(\rho c_p)_{\text{f}} v_\infty \Delta T_{\text{ref}}]. \end{aligned} \tag{8}$$

Eq. (7) become:

$$\nabla^* \cdot v^* = 0; \quad \frac{\mathrm{d}v^*}{\mathrm{d}t^*} = -\nabla^* \hat{p}^* + \frac{1}{Re} \nabla^* 2v^* \quad \text{in } \Omega^*_{\text{f}} \tag{9a}$$

$$\frac{\mathrm{d}T^*_{\text{f}}}{\mathrm{d}t^*} = \frac{\partial T^*_{\text{f}}}{\partial t^*} + v^* \cdot \nabla^* T^*_{\text{f}} = \frac{1}{RePr} \nabla^* \cdot \nabla^* T^*_{\text{f}} + s^*_{\text{f}} \quad \text{in } \Omega^*_{\text{f}} \tag{9b}$$

$$\frac{\partial T^*_{\text{s}}}{\partial t^*} = \frac{1}{RePr} \frac{(\rho c_p)_{\text{f}}}{(\rho c_p)_{\text{s}}} \frac{\lambda_{\text{s}}}{\lambda_{\text{f}}} \nabla^* \cdot \nabla^* T_{\text{s}} + \frac{(\rho c_p)_{\text{f}}}{(\rho c_p)_{\text{s}}} s^*_{\text{s}} \quad \text{in } \Omega^*_{\text{s}} \tag{9c}$$

$$T^*_{\text{s}} = T^*_{\text{f}} \quad \text{and} \quad -\frac{\lambda_{\text{s}}}{\lambda_{\text{f}}} \nabla^* T^*_{\text{s}} \cdot \boldsymbol{n}_{\text{s}} = -\nabla T^*_{\text{f}} \cdot \boldsymbol{n}_{\text{s}} \quad \text{on } \partial\Omega^*_{\text{sf}} \tag{9d}$$

$$T^*_{\text{s}} - T^*_{\text{f}} \to 0 \quad \text{and} \quad T^*_{\text{s}} \to 0 \quad \text{as } \|r^*\| \to \infty \tag{9e}$$

$$T^*_{\text{s}} = T^*_{\text{f}} = 0 \quad \text{at} \quad t^* = 0 \text{ in } \quad \Omega^* = R^3 = \Omega^*_{\text{f}} U \Omega^*_{\text{s}} \tag{9f}$$

where Re_d is the particulate Reynolds number, Pr the Prandtl number, and $\frac{\mathrm{d}}{\mathrm{d}t}$ the material derivative. The solution of the previous system (9) can be written under the formal form:

$$T^*(\boldsymbol{r}^*, t^*) = \int_{t'^*=0}^{\infty} \int_{\boldsymbol{r}'^* \in \Omega^*} f_{\text{loc}}(\boldsymbol{r}^*, t^* | \boldsymbol{r}'^*, t'^*; \ \beta) s^*_{\text{loc}}(\boldsymbol{r}'^*, t'^*) \mathrm{d}\boldsymbol{r}'^* \mathrm{d}t'^*, \tag{10}$$

where $T^* = T^*_{\text{f}}$ and $s^*_{\text{loc}} = s^*_{\text{f}}$ if $r^* \in \Omega^*_{\text{f}}$ and $T^* = T^*_{\text{s}}$ and $s^*_{\text{loc}} = s^*_{\text{s}}$ if $r^* \in \Omega^*_{\text{s}}$.

$\beta = (Re_d, Pr, \lambda_{\text{s}}/\lambda_{\text{f}}, (\rho c_p)_{\text{s}}/(\rho c_p)_{\text{f}})$ is a vector that gathers the four non-dimensional parameters that are present in system (9). Eq. (10) shows that the reduced temperature can be calculated through a space and time integration of the product of the reduced volumetric heat source s^*_{loc} and f_{loc}, which is the corresponding Green's function of the system [16]. It comes from the fact that the fluid flow problem (9a), with initial and external boundary conditions, which can be non-linear, is first solved to yield the reduced velocity field v^*. This steady state field is present simply as a structural non-uniform coefficient in the linear heat equation system (9(a)–(f)) whose source term is s^*_{loc}. In our case, all the thermophysical coefficients are constant, which means that the time integral becomes a convolution product in time in the case of a steady state flow (time invariant system).

The definition (1) of the average enthalpic temperature of the one-temperature model can be re-written using Eq. (10) after inversion of the order of the averaging operator and of the space and time integration, which yields:

$$\begin{aligned} T_H(\boldsymbol{r}, t) = T_{\text{ref}} + \frac{\Delta T_{\text{ref}}}{(\rho c_p)_{\text{t}}} \int_{t'^*=0}^{\infty} \int_{\boldsymbol{r}'^* \in \Omega^*} \\ \times \langle \rho c_p(\boldsymbol{r}'') f_{\text{loc}}(\boldsymbol{r}''^*, t^* | \boldsymbol{r}'^*, t'^*; \beta) \rangle s^*_{\text{loc}}(\boldsymbol{r}'^*, t'^*) \mathrm{d}\boldsymbol{r}'^* \mathrm{d}t'^*. \end{aligned} \tag{11}$$

Another reduction of Eq. (3) whose solution is the same average temperature will be introduced now. It can be made using the mesoscopic length scale D, the same reference velocity v_∞, and the same reference temperature difference $\Delta T_{\text{ref}} = T_0 - T_{\text{ref}}$. The new dimensionless quantities are then:

$$\begin{aligned} &\boldsymbol{r}^\circ = \boldsymbol{r}/D = (d/D)\boldsymbol{r}^*; \quad \boldsymbol{u}^\circ_D = \boldsymbol{u}_D/v_\infty; \\ &t^\circ = v_\infty t/D = (d/D)t^*; \quad T^\circ_H = (\langle T \rangle - T_{\text{ref}})/\Delta T_{\text{ref}}; \\ &s^\circ = Ds/[(\rho c_p)_{\text{f}} v_\infty \Delta T_{\text{ref}}] = (D/d)s^* \end{aligned} \tag{12}$$

where s^* corresponds to the same normalization as s^*_{loc}, s^*_{f} and s^*_{s} in (8) and (10). With this new reduction, it is possible to write a reduced form of (3):

$$\frac{\partial T^\circ_H}{\partial t^\circ} = \nabla^\circ \left(\frac{1}{(\rho c_p)_{\text{t}} v_\infty D} \lambda \nabla^\circ T^\circ_H \right) - \frac{(\rho c_p)_{\text{f}}}{(\rho c_p)_{\text{t}}} \boldsymbol{u}^\circ_D \nabla^\circ T^\circ_H + s^\circ. \tag{13}$$

Coming back to the non-reduced average temperature, we get the following form for the solution of (13) with the same reference temperature, initial and boundary ($r \to \infty$) conditions:

$$\begin{aligned} T_H(\boldsymbol{r}, t) = T_{\text{ref}} + \Delta T_{\text{ref}} \int_{t'^\circ=0}^{\infty} \\ \times \int_{\Omega^\circ} k_{\text{ave}}(\boldsymbol{r}^\circ, t^\circ | \boldsymbol{r}'^\circ, t'^\circ; \boldsymbol{u}^\circ_D, \alpha) s^\circ(\boldsymbol{r}'^\circ, t'^\circ) \mathrm{d}\boldsymbol{r}'^\circ \mathrm{d}t'^\circ \end{aligned} \tag{14}$$

with:

$$\alpha = \left(\frac{1}{(\rho c_p)_{\text{t}} v_\infty D} \lambda, (\rho c_p)_{\text{f}}/(\rho c_p)_{\text{t}} \right) \tag{15}$$

k_{ave} being the corresponding Green's function. It is possible to make the same reduced integration variables as in Eq. (11) appear, which yields

$$T_H(r,t) = T_{\text{ref}} + \Delta T_{\text{ref}} \int_{t'^*=0}^{\infty} \int_{\Omega^*} m_{\text{ave}}(\boldsymbol{r}^*, t^* | \boldsymbol{r}'^*, t'^*; \gamma) s^*(\boldsymbol{r}'^*, t'^*) \mathrm{d}\boldsymbol{r}'^* \mathrm{d}t'^* \tag{16}$$

with:

$$m_{\text{ave}} = \frac{d^3}{D^3} k_{\text{ave}} \left(\frac{d}{D}\boldsymbol{r}^*, \frac{d}{D}t^* \middle| \frac{d}{D}\boldsymbol{r}'^*, \frac{d}{D}t'^*; \boldsymbol{u}^\circ_D, \alpha \right) \quad \text{and} \quad \gamma = \left(\frac{\boldsymbol{u}_D}{v_\infty}, \frac{d}{D}, \alpha \right)$$

Comparison of Eq. (16) with Eq. (11), which should give the same average temperature for any point $P(\boldsymbol{r})$ at any

time t, under the assumption that the one-temperature model is valid for a given configuration (porous medium, flow and source), leads to the following identity for the ratio s/s_{loc} of the source terms:

$$\frac{s(\boldsymbol{r}',t')}{s_{\mathrm{loc}}(\boldsymbol{r}',t')}=\frac{\langle\rho c_p f_{\mathrm{loc}}\rangle(\boldsymbol{r}^*,t'^*,\beta)}{(\rho c_p)_{\mathrm{t}}m_{\mathrm{ave}}(\boldsymbol{r}^*,t^*|\boldsymbol{r}'^*,t'^*;\gamma)}. \tag{17}$$

For energy conservation reasons the left hand member of this equation should be equal to unity if the one-temperature model is pertinent. As a consequence, one can write the following identity:

$$m_{\mathrm{ave}}(\boldsymbol{r}^*,t^*|\boldsymbol{r}'^*,t'^*;\gamma)=\frac{1}{(\rho c_p)_{\mathrm{t}}}\langle\rho c_p f_{\mathrm{loc}}\rangle(\boldsymbol{r}^*,t'^*,\beta). \tag{18}$$

In the case of a plug flow in the x direction in a homogeneous porous medium the filtration velocity $\boldsymbol{u}_D$ is uniform and, consequently, the reduced filtration velocity $\boldsymbol{u}_D/v_\infty$ can be removed from the arguments of γ in m_{ave}. As a consequence, the different components of the γ parameter vector present in the left-hand side of Eq. (18) must depend on their counterparts in β in the right hand side and, in particular:

$$\frac{1}{(\rho c_p)_{\mathrm{t}}v_\infty D}\lambda=\boldsymbol{k}(Re_d,Pr,\lambda_{\mathrm{s}}/\lambda_{\mathrm{f}},(\rho c_p)_{\mathrm{s}}/(\rho c_p)_{\mathrm{f}}), \tag{19}$$

where $\boldsymbol{k}$ is a vector function, which represents the variation of the three principal dispersion coefficients of the dispersion tensor. It depends on the location of the $\partial\Omega_{\mathrm{sf}}$ interface between the solid and fluid phases. This means that, strictly speaking, this function is attached to a particular structure of the porous medium and to a particular value of the ratio between the characteristic and averaging lengths d/D. We focalize here on the case where the structure of the granular medium is isotropic (case of a bed of spherical or of ellipsoidal grains with random principal axes for example). In these cases, if x is the direction of the plug flow, the dispersion tensor is fully characterized by a longitudinal component λ_x and a unique $\lambda_y=\lambda_z$ transverse or lateral component.

Eq. (19) can be multiplicated by the particulate Péclet number $Pe=Re_dPr$, which yields

$$\frac{d}{D}\frac{(\rho c_p)_{\mathrm{f}}}{(\rho c_p)_{\mathrm{t}}}\frac{\lambda}{\lambda_{\mathrm{f}}}=Re_dPr\;\boldsymbol{k}(Re_d,Pr,\lambda_{\mathrm{s}}/\lambda_{\mathrm{f}},(\rho c_p)_{\mathrm{s}}/(\rho c_p)_{\mathrm{f}}) \tag{20}$$

or

$$\lambda_{x\,\mathrm{or}\,y}/\lambda_{\mathrm{f}}=g_{x\,\mathrm{or}\,y}(Re_d,Pr,\lambda_{\mathrm{s}}/\lambda_{\mathrm{f}},(\rho c_p)_{\mathrm{s}}/(\rho c_p)_{\mathrm{f}},d/D). \tag{21}$$

At this point we consider the limiting case where the d/D ratio is small enough, which yields:

$$\lambda_{x\,\mathrm{or}\,y}/\lambda_{\mathrm{f}}=g_{x\,\mathrm{or}\,y}(Re_d,Pr,\lambda_{\mathrm{s}}/\lambda_{\mathrm{f}},(\rho c_p)_{\mathrm{s}}/(\rho c_p)_{\mathrm{f}}). \tag{22}$$

Function g (for the longitudinal x or transverse y dispersion coefficient) represents the correlation that is to be sought to explain thermal dispersion in an infinite homogeneous porous medium, that is far from the macroscopic walls. Its arguments are linked to the filtration velocity, to the fluid viscosity and to the thermal properties of the fluid and solid phases. However, a priori, this function has to be changed if the structure of the granular medium is changed (change of granulometry or change of the shape of the grains). An interesting way to describe this structural dependence is to make the equivalent conductivity λ_{eq} of the homogenized medium, appear. This conductivity is given in the last two columns of Table 1, for two solid/fluid systems. Eq. (22) is thus written, for a zero velocity, which also makes the Prandtl number and the volumetric capacity ratio disappear:

$$\lambda_{\mathrm{eq}}/\lambda_{\mathrm{f}}=g_x(Re_d=0,\lambda_{\mathrm{s}}/\lambda_{\mathrm{f}})=g_y(Re_d=0,\lambda_{\mathrm{s}}/\lambda_{\mathrm{f}})=g_0(\lambda_{\mathrm{s}}/\lambda_{\mathrm{f}}). \tag{23}$$

Combination of Eqs. (22) and (23) yields:

$$\lambda_{x\,\mathrm{or}\,y}/\lambda_{\mathrm{eq}}=f_{x\,\mathrm{or}\,y}(Re_d,Pr,\lambda_{\mathrm{s}}/\lambda_{\mathrm{f}},(\rho c_p)_{\mathrm{s}}/(\rho c_p)_{\mathrm{f}}). \tag{24}$$

Function g_0 does not depend on the conductivity ratio only but also on the structure of the porous medium. The effect of the structure can be expressed by a model where the porosity is present explicitly, see [2] for example. One can expect consequently that function $f_{x\,\mathrm{or}\,y}$ depends less on the structure of the medium and on the $\lambda_{\mathrm{s}}/\lambda_{\mathrm{f}}$ ratio than function $g_{x\,\mathrm{or}\,y}$.

The preceding forms of the correlations for the dispersion coefficients were derived under the assumption of a pertinent one-temperature model. The limits of this model is studied in Appendix A, starting from a two-temperature model [17]: it is shown that the use of the one-temperature model is legitimate in our experimental configuration.

5. Parameter estimation technique and simulation of inversion

A least square technique has been used here to estimate the dispersion coefficients λ_x and λ_y present in the theoretical model (6) for a given filtration velocity u, starting from temperature measurements produced by several thermocouples located downstream the heating wire. The corresponding experimental thermograms are plotted in Fig. 3(a) (water/glass beads) and Fig. 3(c) (air/glass beads) for thermocouples 2–7, see Fig. 1. In order to know whether this estimation is possible, it is very interesting to study the time variation of the reduced sensitivities β_jX_j of temperature to the different β_j parameters of the problem [18], with

$$\beta=[\,\lambda_x\quad\lambda_y\quad u\,]^{\mathrm{t}}\quad\text{and}\quad X_j=\frac{\partial T}{\partial\beta_j}. \tag{25}$$

The reduced sensitivity coefficients β_jX_j as well as the reduced sensitivities to the two coordinates of thermocouple 2, LX_x and LX_y, with $L=1$ cm, are plotted in Fig. 2(a) and (b) (water flow) and (air flow). These sensitivities correspond to the same Péclet number $Pe=9.06$ for an excitation $Q=70$ W/m (water case) or $Q=7.5$ W/m (air case).

The sensitivities of the water case, Fig. 2(a), are first discussed. It is very clear that, at this location, the sensitivities

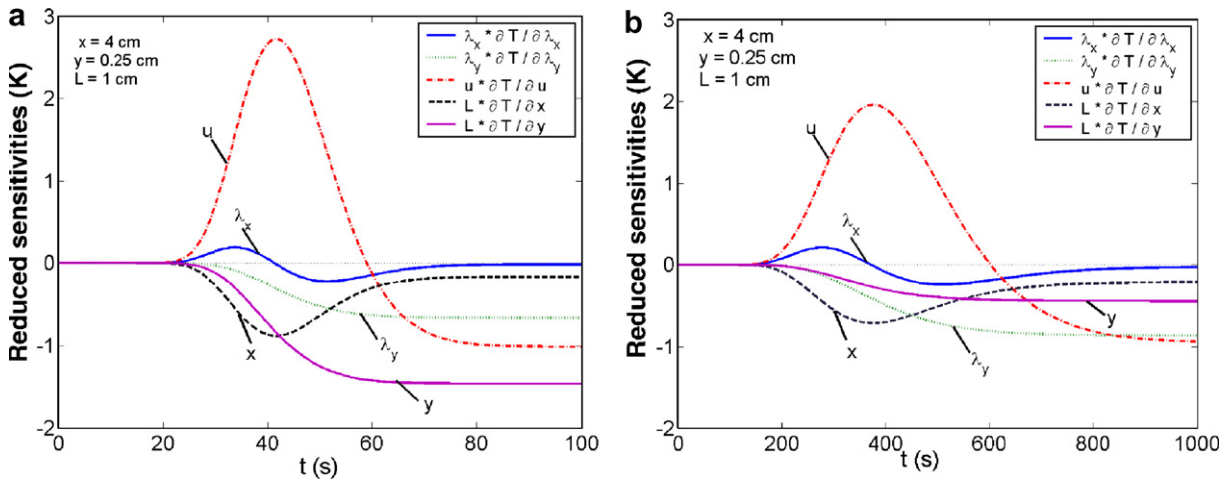

Fig. 2. Relative sensitivities. (a) Water flow; $Pe = 9.06$; $Q = 70$ W/m; $\lambda_x = 2.4$ W m^{-1} K^{-1}; $\lambda_y = 1$ W m^{-1} K^{-1}; $u = 0.655$ mm/s. (b) Air flow; $Pe = 9.06$; $Q = 7.5$ W/m; $\lambda_x = 0.26$ W m^{-1} K^{-1}; $\lambda_y = 0.19$ W m^{-1} K^{-1}; $u = 9.7$ cm/s.

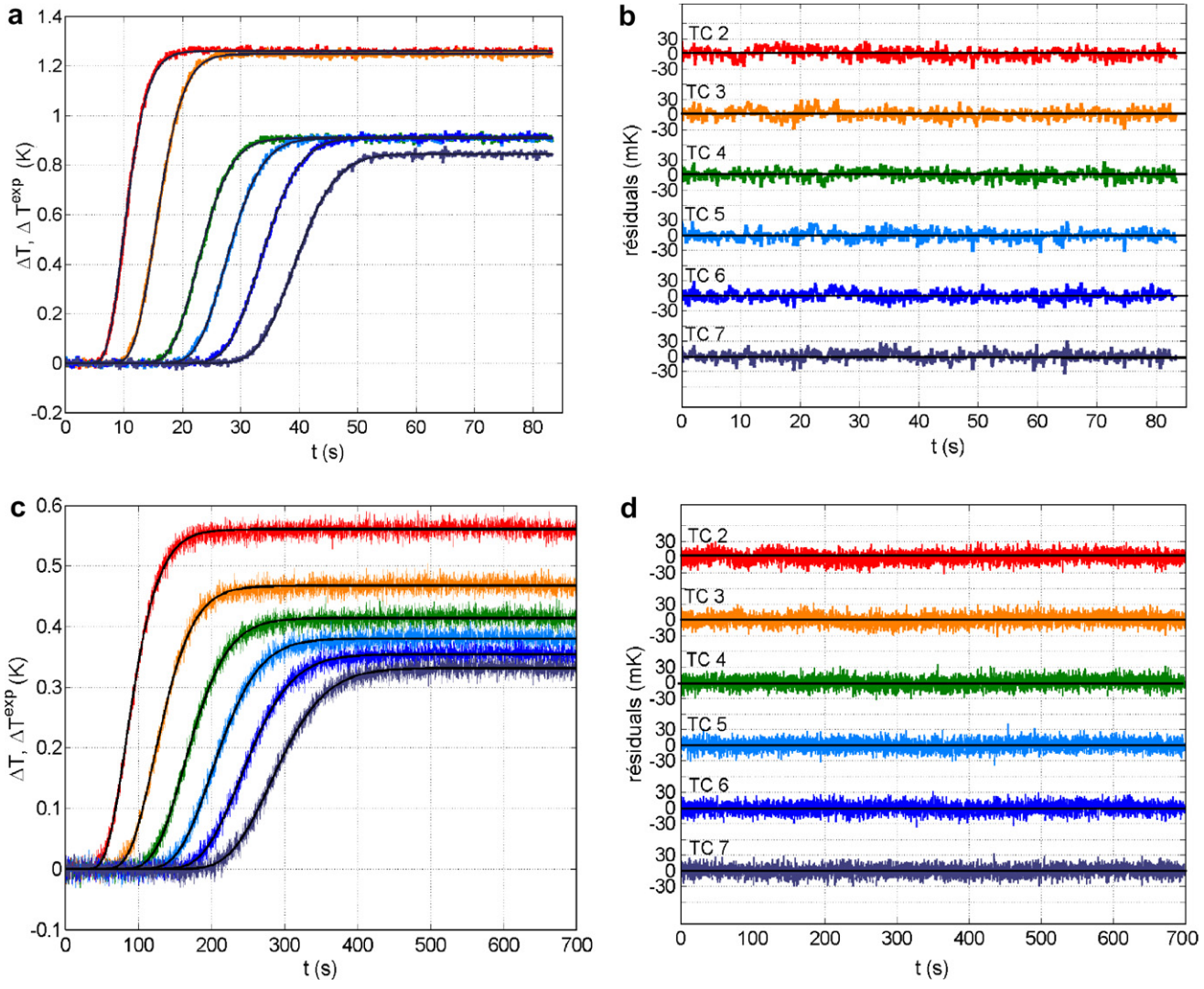

Fig. 3. Transient temperature responses and residuals for water and air flows for $Pe \cong 30$. (a) Experimental and reconstructed responses, water flow; (b) temperature residuals, water flow; (c) experimental and reconstructed responses, air flow; (d) temperature residuals, air flow.

of temperature to velocity u and to location y are the highest. Let us note that Eq. (6) shows the sensitivity to this y-location is equal to zero if the temperature is measured in the symmetry axis ($y = 0$). One can also notice that sensitivities to λ_y and to y are nearly proportional. The same is true for sensitivities to u and to x, for short times only, but these times bring most of the information on the different parameters. This means that, without any information on the exact location of the thermocouples, it will not be possible to estimate the β parameters. The same is true if more than one thermocouple is used for inversion because of the addition of new location parameters. The different sensitivities of the air case shown in Fig. 2(b) vary in the same manner, but one can notice that sensitivity to the y location is now lower than sensitivity to λ_y. This means that the uncertainty in the y-position of the thermocouples will be less penalizing for the estimation of the transverse dispersion coefficient than in the water case. Such a problem caused a very rough estimation of λ_y on the same set-up in the water case [10].

We briefly recall here the estimation technique already used by Metzger et al. [10,19]. In order to take into account the uncertainty in the exact (x_i, y_i) location of thermocouple number i, that may differ from its nominal (x_i^{nom}, y_i^{nom}) location, a penalized least squares sum has been minimized here (Baye's inversion):

$$S(\alpha) = \frac{1}{\sigma_T^2}\sum_{i=1}^{Nt_c}\sum_{k=1}^{Nt}\left(T_{\text{exp},ik} - T_{ik}(\alpha)\right)^2 + \frac{1}{\sigma_{\text{loc}}^2}\sum_{i=1}^{Nt_c}\left(x_i^{\text{nom}} - x_i\right)^2 + \frac{1}{\sigma_{\text{loc}}^2}\sum_{i=1}^{Nt_c}\left(y_i^{\text{nom}} - u_i\right)^2 \quad (26)$$

where $\alpha = [\lambda_x, \lambda_y, u, (x_i, y_i)_{i=1,Nt_c}]^t$ is the new extended parameter vector to be estimated, Nt_c the number of thermocouples used (thermocouples 2–7 here, see Fig. 1) and Nt the number of measurement times. $T_{\text{exp},ik}$ is the temperature measured at the (exact) location of the ith thermocouple and t_k, the kth time of measurement. $T_{ik}(\alpha) = T(x_i, y_i, z_i, t_k; \beta)$ is the corresponding theoretical temperature given by Eq. (6)

The experimental temperature standard deviation σ_T can be measured in a steady state situation ($\sigma_T =$ 0.02 °C), that is without any excitation Q, and it can be assumed that the standard deviation of the location of a hot junction, that is a measure of its displacement, is of the order of one bead radius ($\sigma_{\text{loc}} = 1$ mm).

In order to assess the quality of the estimation and to study the effect of the temperature and location noise on the estimator obtained by minimization of sum (26), it is very interesting to implement it on synthesized measurements, that is to use a Monte Carlo process: the exact temperature response of model (6) is noised with an independent additive normal random noise of zero mean and standard deviation σ_T, which yields the simulated experimental temperatures $T_{\text{exp},ik}$. The same technique is implemented with both exact thermocouple coordinates (x_i, y_i) that are noised in the same way with a noise of standard deviation σ_{loc} to produce the nominal locations (x_i^{nom}, y_i^{nom}). A Gauss-Newton minimization of S yields an estimation $\hat{\alpha}$ of the parameter vector α. If 400 simulations of this type are made with the corresponding inversions, 400 estimates $\hat{\alpha}_j^{(n)}$ are available for the jth parameter of $\hat{\alpha}$, n being the inversion number. It is then possible to reach the statistical distribution of each estimated parameter (its histogram) and to calculate the dispersion (standard deviation s_j) of each estimate as well as its bias b_j, that are:

$$b_j = \bar{\hat{\alpha}}_j - \alpha_j \quad \text{and}$$

$$s_j = \frac{1}{400}\sum_{n=1}^{400}\left(\hat{\alpha}_j^{(n)}\right)^2 - \left(\bar{\hat{\alpha}}_j\right)^2 \quad \text{with} \quad \bar{\hat{\alpha}}_j = \frac{1}{400}\sum_{n=1}^{400}\hat{\alpha}_j^{(n)}. \quad (27)$$

Such estimates are given in Table 2 for air or water flow through the glass beads. They correspond to the positions of thermocouples 2–7 located at $x = 4$, 6, 8, 10, 12 and 14 cm with an off-axis displacement $y = 2.5$ mm, and to a time step of 0.15 s, with a final time of 900 s for air, the corresponding values being 0.15 s and 45 s for water. One can use here the $(|b_j| + s_j)/\alpha_j$ ratio (relative error) as an index of quality of inversion for parameter α_j.

The λ_x estimations have the same quality for air and water with 'relative errors' smaller than 3%: bias is larger for air but it is compensated by a lower dispersion. For the λ_y estimations the 'relative error' is still acceptable for air (5%) but too large for water (21%) to yield precise values; this explains the low precision estimation of λ_y already mentioned above [10]. For both fluids the filtration velocity is the parameter that is estimated with the maximum precision (relative errors lower than 2%). This confirms the possibility of estimating the transverse dispersion coefficient

Table 2
Monte Carlo simulations of inversion for air or water flow through a bed of glass beads

	j	Parameter	Exact value α_j	Average estimation $\bar{\hat{\alpha}}_j$	Estimation bias b_j	Estimation standard deviation s_j	Bias/dispersion $\lvert b_j\rvert/s_j$	Relative error $(\lvert b_j\rvert + s_j)/\alpha_j$
Air	1	λ_x (W K^{-1} m^{-1})	0.962	0.984	+0.022	0.008	275%	3%
	2	λ_y (W K^{-1} m^{-1})	0.256	0.246	−0.010	0.003	336%	5.2%
	3	u (m s^{-1})	0.353	0.355	+0.002	0.004	50%	1.7%
Water	1	λ_x (W K^{-1} m^{-1})	60	60.321	+0.321	1.009	32%	2.2%
	2	λ_y (W K^{-1} m^{-1})	3	2.681	−0.329	0.310	106%	21%
	3	u (mm s^{-1})	6.288	6.306	+0.018	0.033	55%	0.8%

with a very good precision for air, and with a lower precision for water.

In this problem, the estimation bias on the different parameters caused by the non linear character of the estimator can become higher than its standard deviation, see the $|b_j|/s_j$ column in Table 2.

6. Experimental estimation of the dispersion coefficients

The experimental and recalculated thermograms (thermocouples 2–7) as well as the temperature residuals are shown in Fig. 3(a) and (b) for water flow and in Fig. 3(c) and (d) for air flow through the 2 mm glass beads. The Péclet numbers are close for the two cases ($Pe \cong 30$). The temperature residuals ($T_{\exp,ik} - T_{ik}(\alpha)$) are plotted as functions of time for each thermocouple.

Their quadratic mean is lower than 30 mK and identical for the two fluids. The low level and the non correlated shape of the residuals show that the one-temperature model fits very well the experimental curve for both flows. One can notice that the measurement duration is about 10 times larger for air than for water. This can be explained by the fact that the energy equation of the one-temperature model can be normalized by its division by the total heat capactity $(\rho c_p)_t$ to make a corrected velocity $u^* = (\rho c_p)_f u/(\rho c_p)_t$ appear. For a same Péclet number for air and water flow through the same bed, the ratio of the corresponding corrected velocities become:

$$\frac{u^*_{\text{water}}}{u^*_{\text{air}}} = \frac{\lambda_{\text{water}}}{\lambda_{\text{air}}} \frac{(\rho c_p)_{\text{t air/glass}}}{(\rho c_p)_{\text{t water/glass}}} \approx 10. \tag{28}$$

7. Experimental correlations for the dispersion coefficients

7.1. The longitudinal dispersion coefficient

Experiments have been made with water flow through 2 mm diameter glass beads and with air flow through 2 and 3 mm diameter glass beads. The measured porosity of the beds is $\varepsilon = 0.365$. For both cases the velocity has been estimated from inversion of the temperature measurements and the particulate Reynolds or Péclet numbers have been constructed with the corresponding bead diameter d. Usually experimental correlations for the dispersion coefficients present the variation of this coefficients with the Péclet number $Pe = RePr$, that is the only reduced number present in the fluid phase reduced energy equation. This presentation is legitimate if dispersion results concerning only one single fluid are given. The experiments presented here correspond to completely different intervals of Reynolds number and consequently to different flow regimes in the porous medium. They are in the 0.5–18 range for water, which corresponds to the Darcy regime while they are in the 12–110 range for air flow, which corresponds to the inertial regime described by Forcheimer's equation, that starts for Reynolds number between 1 and 10 for a three-dimensional flow around spheres [12]. So, a Péclet number of 30 corresponds to a Reynolds number around 4.3 for water (Darcy regime) and close to 43 for air (inertial regime). The experimental variations of the estimations of λ_x with the fluid (water or air) Reynolds number Re are shown in Fig. 4(a) (normalization by the fluid conductivity). The estimates have not been subjected to any bias correction here. One can notice that the dispersion of the estimations of λ_x agrees with the theoretical Monte Carlo simulations shown in Table 2, even if some extra dispersion is probably due to slight temperature variations of the incoming air depending on the day the experiment was made. These ambient temperature variations can have an effect on both water and air conductivities whose ratio appear in the form of the correlation (22) giving λ_x/λ_f. One can verify that the size of the beads has no effect on dispersion in air.

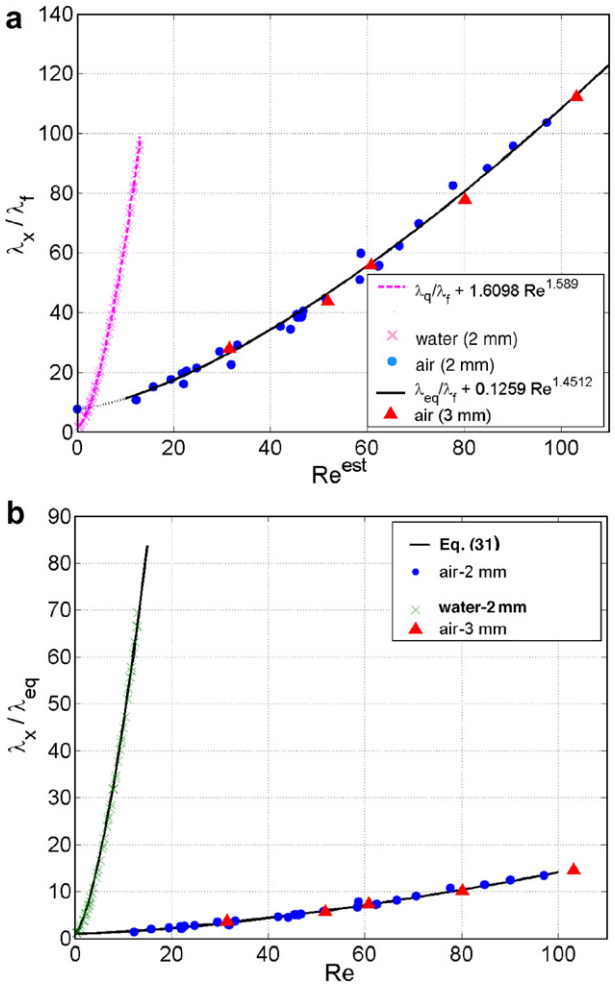

Fig. 4. Estimation results for the longitudinal dispersion coefficient (water– and air–glass beads systems): Effect of the Reynolds number (a) normalization by the fluid conductivity; (b) normalization by the equivalent conductivity of the homogenized medium and unique correlation for both fluids.

We have modelled our results in water by a power law correlation [10,19]:

$$\frac{\lambda_x}{\lambda_f} = \frac{\lambda_{eq}}{\lambda_f} + 0.0731 Pe^{1.59} = \frac{\lambda_{eq}}{\lambda_f} + 1.61 Re^{1.59}$$
$$\text{for} \quad 0 < Re < 18 \quad \text{and} \quad Pr = 7.02. \tag{29}$$

A correlation of a similar form can be found for the air results [20]:

$$\frac{\lambda_x}{\lambda_f} = \frac{\lambda_{eq}}{\lambda_f} + 0.211 Pe^{1.45} = \frac{\lambda_{eq}}{\lambda_f} + 0.126 Re^{1.45}$$
$$\text{for} \quad 12 < Re < 130 \quad \text{and} \quad Pr = 0.7. \tag{30}$$

It is interesting to notice here that the constraint that was put on both correlations to pass through the point at zero velocity $\lambda_x = \lambda_{eq}$ does not seem to distort the corresponding curves.

The preceding results for the water/glass beads and air/glass beads systems are in the [0;130] range of Reynolds number. It is possible to look for a unique correlation of the form (24) for both systems: this correlation must also be valid for a zero velocity where $\lambda_x = \lambda_y = \lambda_{eq}$:

$$\frac{\lambda_x}{\lambda_{eq}} = 1 + \frac{\lambda_f}{\lambda_{eq}} \varepsilon(1-\varepsilon) Re^{1.5} \left[\frac{8.87(Pr-0.7) - 0.543(Pr-7.02)}{6.32} \right]. \tag{31}$$

This correlation has been constructed through a linear interpolation of Eqs. (29) and (30) with respect to the Prandtl number of the fluid phase, with a fixed 1.5 exponent for the Reynolds number that lies in-between the water (1.59) and air (1.45) exponents. The porosity factor $\varepsilon(1-\varepsilon)$ in the second term of the right-hand member makes this correlation valid for pure fluids ($\varepsilon = 1$, $\lambda_x = \lambda_y = \lambda_{eq} = \lambda_f$) and for pure solids ($\varepsilon = 0$, $\lambda_x = \lambda_y = \lambda_{eq} = \lambda_s$). One weakness of this correlation concerns the absence of the volumetric capacity ratio of the two phases in the arguments present in its right-hand member. Only experiments with different solid/fluid pairs would be able to precise this dependence. Both the experimental points for air and water as well as the previous correlation (31) have been plotted in Fig. 4(b). The correlation models our measured points in a satisfactory way.

Another interesting way of presenting the dispersion results consists in plotting the dynamic part ($\lambda_x - \lambda_{eq}$) of the dispersion coefficient, normalized by the fluid conductivity λ_f, as a function of the particulate Péclet number for both systems. Such a presentation is shown in Fig. 5(a).

In this Péclet representation the relative effect of the Péclet number on the dynamic component of the longitudinal dispersion coefficient seems to be greater for air than for water flow. Normalization by the equivalent conductivity would imply the opposite conclusion.

Fig. 5(b) shows a comparison of our experimental results for the longitudinal dispersion coefficient for the air/glass beads system (2 mm diameter), plotted versus the Péclet number, with Tsotas's model [5], Levec and Carbonell's correlation [7] and the experimental results of Gunn et al. [4] and Yagi et al. [1] for the same system. Apart from Gun's

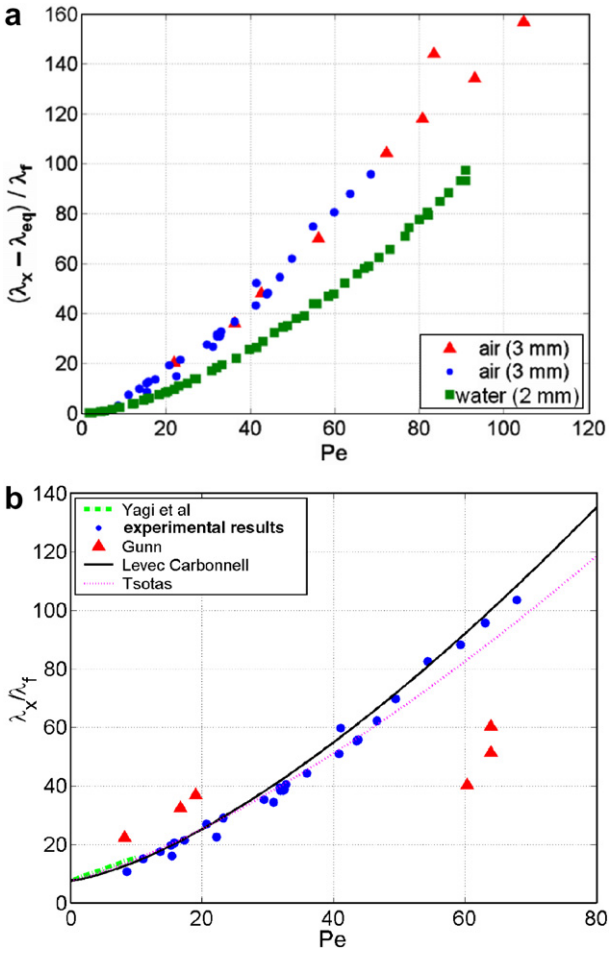

Fig. 5. Estimation results for the longitudinal dispersion coefficient normalized by the fluid conductivity, effect of the Péclet number: (a) dynamic contribution, water– and air–glass beads systems (b) comparison with literature data, air–glass beads systems.

results, all the previous data agree very well with ours for Péclet numbers up to 50. Beyond this value Levec and Carbonell's correlation is very close to our results.

7.2. The lateral dispersion coefficient

The experimental estimations of the lateral dispersion coefficient, normalized here with the air conductivity, are plotted versus the particulate Reynolds number in Fig. 6(a). One can verify that the diameter of the beads, 2 or 3 mm, has no effect on the dispersion coefficient in this representation.

A corresponding correlation has been looked for under the following form:

$$\frac{\lambda_y}{\lambda_f} = A_y + B_y Re = 6.40 + 0.0788 Re = 6.40 + 0.113 Pe$$
$$\text{for} \quad 12 < Re < 130 \quad \text{and} \quad Pr = 0.7. \tag{32}$$

One can notice here that, contrary to what has been done in Section 7.1, the correlation has not been imposed to go through the point corresponding to a zero velocity

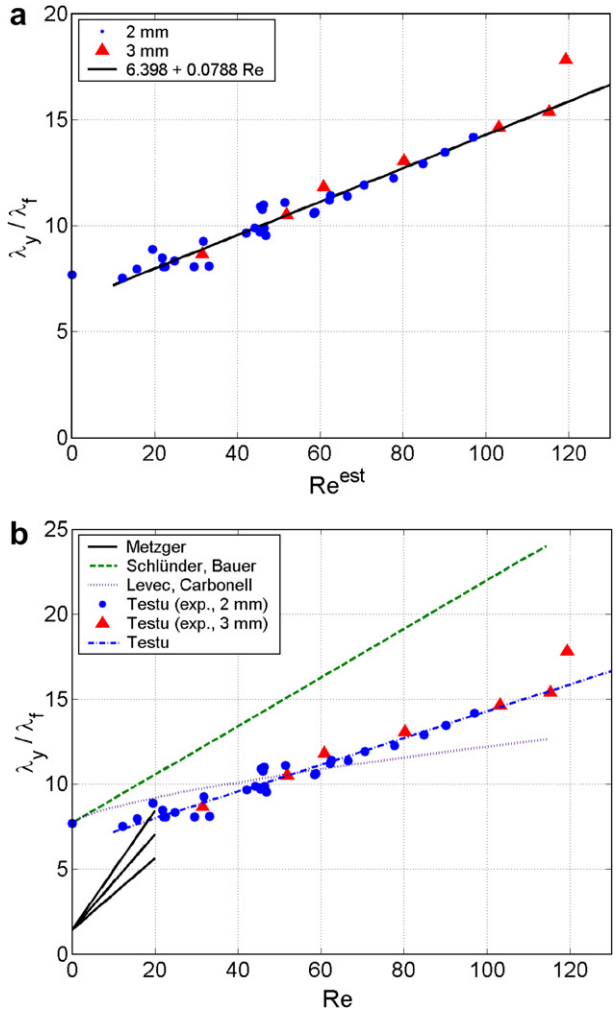

Fig. 6. Estimation results for the lateral dispersion coefficient normalized by the fluid conductivity, effect of the Reynolds number: (a) air–glass beads systems; (b) comparison with literature data, water– and air–glass beads systems.

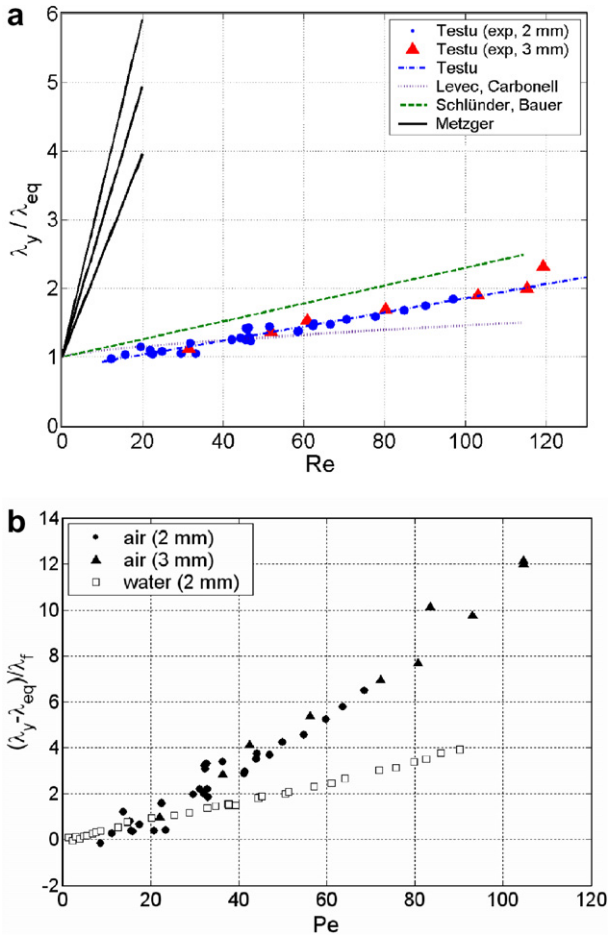

Fig. 7. Comparison between water– and air–glass beads lateral dispersion results; (a) normalization by the homogenized medium equivalent conductivity, effect of the Reynolds number; (b) dynamic contribution, normalization by fluid conductivity, effect of the Péclet number.

($A_y \neq \lambda_{eq}/\lambda_f$). This correlation is valid only for Reynolds numbers higher than 12. One can note that λ_y and λ_{eq} are nearly equal for a Reynolds number equal to 12. Since the equivalent conductivity λ_{eq} of the air/glass bead system is well known, it seems probable that the lateral dispersion coefficient λ_y does not differ much from its static value λ_{eq} for Reynolds numbers lower than 12. This effect is specific to the Darcy regime in the porous medium (or to the Stokes regime in its fluid phase): in this regime the shape of the streamlines does not vary with the flow rate level [12]. This flow property could be related to the fact that the lateral dispersion coefficient keeps its static value, even if this link remains to be explained.

We have plotted our λ_y results, normalized by the fluid conductivity, see Fig. 6(b), or by the equivalent conductivity of the fluid/glass beads system, see Fig. 7(a), as well as those of Bauer and Schlünder [6] and Levec and Carbonnel models [7] for the air/glass beads systems. The experimental results by Metzger et al. [10] for a water/glass beads system are also plotted.

Mezger's results, whose precision is lower than the air/glass beads results, correspond to the following correlation:

$$\frac{\lambda_y}{\lambda_f} = \frac{\lambda_{eq}}{\lambda_f} + C_y RePr \quad \text{with} \quad C_y = 0.04 \pm 0.01$$
$$\text{for} \quad 0.5 < Re < 18 \quad \text{and} \quad Pr = 7.02. \tag{33}$$

One clearly sees that, for the same Reynolds number, lateral dispersion for a water flow exhibits a completely different behaviour than for an air flow. It is also clear that Bauer and Schlünder overestimate our results while it is the opposite for Levec and Carbonnel, but only for Reynolds numbers over 50.

The dynamic part ($\lambda_y - \lambda_{eq}$) of the estimation of the lateral dispersion coefficient, normalized by the fluid conductivity λ_f, as a function of the particulate Péclet number for both systems is plotted in Fig. 7(b). The air/glass curve represents the results of this work while the water /glass curve represents the best estimations for the water glass experimental results of Metzger [10]. These results were obtained for a thermocouple whose location residuals (x, y) were very low. When compared to the same representation for

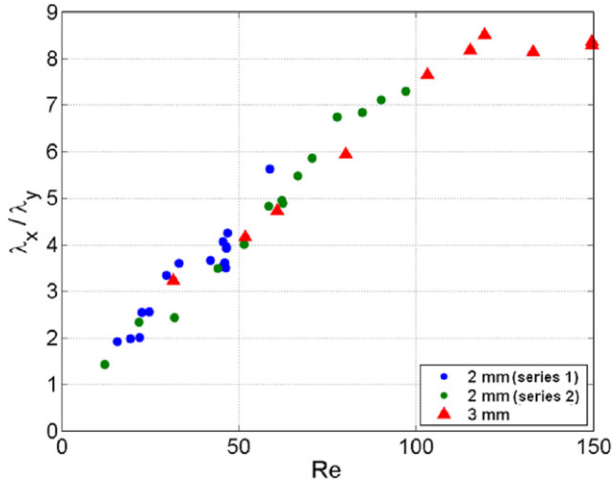

Fig. 8. Anisotropy ratio of the thermal dispersion coefficients λ_x/λ_y for the air/glass beads system.

longitudinal dispersion, see Fig. 5(a), one clearly sees that the velocity effect is clearly lower for lateral dispersion.

The anisotropy effect of the thermal dispersion tensor, that is the variation of the λ_x/λ_y for the air/glass beads system with the Reynolds number, is presented in Fig. 8. This variation seems to be linear up to Reynolds numbers close to 80.

8. Conclusions

The thermal dispersion model that uses only one 'enthalpic' average temperature obtained from a up-scaling process has been presented here for an air flow through a bed of glass beads. An experimental configuration has been designed for measuring, by an inverse technique, the two coefficients of this model, the longitudinal and lateral thermal dispersion coefficients. The functional form of the experimental correlations that explain the variation of the dispersion coefficients with the structural and thermophysical properties of the solid and fluid phases of the granular medium, and on the flow velocity, has been established on a theoretical basis. The effect of a possible temperature difference between both phases and on the nature of the output signal of the thermocouple immersed in the granular medium has been scrutinized using a two-temperature model adapted to the granular structure of the porous medium. This study shows that the temperature differences between the two phases can be neglected. The specific inverse estimation technique which allows uncertainties in the locations of the thermocouple hot junctions (Bayes's estimation) has been developed and the estimation errors in terms of standard deviations and bias have been assessed using Monte Carlo simulations of inversion. Two correlations, valid for particulate Reynolds numbers from 12 to 130 have been established. Comparisons have been made with previous similar estimations of the dispersion coefficient for water flow through the same glass beads for Reynolds numbers up to 18. Future work will be devoted to modelling and evaluating experimentally the thermal consequence of the channelling effects near the solid wall limiting the extent of this type of bed using the thermal dispersion correlations that have been developed here for the core region.

Appendix A. Thermal equilibrium problem and Coats–Smith model

In the experiments that were devoted to the estimation of the coefficients, λ_x and λ_y, it has been assumed that the one-temperature model could be used for both water and air flows through glass beads. Temperature measurements corresponding to the configuration presented in Fig. 1 were made using thermocouples, whose hot junctions had a diameter of the order of 0.2 mm. These thermocouples were inserted in-between the glass beads, of diameter $d = 2$, $R = 2$ mm. This means that, rigorously, the measured temperature is the fluid temperature and not the average 'enthalpic' temperature of the one-temperature model defined by (1). One can wonder then whether temperature differences between fluid and solid could build up locally, which could bias our results, in particular in the air flow case where the fluid diffusion time R^2/a_f is a lot shorter than the corresponding time R^2/a_s in the solid phase.

In order to assess the magnitude of this possible temperature desequilibrium, it is possible to use a two-temperature model. This type of model requires the introduction of the intrinsic average temperatures in the fluid and solid phases [21] that are defined below:

$$\langle T_\alpha \rangle^\alpha(P) = \frac{1}{V_\alpha(P,D)} \int_{V_\alpha(P,D)} T(P')\mathrm{d}V(P'), \tag{A.1}$$

where $\alpha = s$ or f and where V_α is the corresponding volume of the α phase in the representative volume of the porous medium, here the sphere of diameter $D(V = V_f U V_s)$, see Section 1. The average 'enthalpic' temperature can be calculated once the two intrinsic average temperatures are known:

$$T_H = \frac{(\rho c_p)_f \varepsilon}{(\rho c_p)_t} \langle T_f \rangle^f + \frac{(\rho c_p)_s (1-\varepsilon)}{(\rho c_p)_t} \langle T_s \rangle^s. \tag{A.2}$$

It is interesting to use here the Coats–Smith model [17], a two-temperature model, to assess the difference between T_s and T_f. This model was derived for mass diffusion in a double porosity porous medium (in the sense of the periodic homogenisation technique), that is a medium where a stagnant fluid volume is present in some part of the porous medium while fluid can flow in its complementary part. An analogous model can be used here for heat transport with pure conduction in the solid grains and convection in the fluid phase. It is assumed here that no volumetric heat source is present in the solid phase. The heat balance

for the fluid phase intrinsic temperature is written in this case:

$$(\rho c_p)_f\left(\varepsilon\frac{\partial\langle T_f\rangle^f}{\partial t}+\boldsymbol{u}_D\cdot\nabla\langle T_f\rangle^f\right)$$
$$=\nabla\cdot(\Lambda_f\nabla\langle T_f\rangle^f)+q_{s\to f}+s\quad\text{in }\Omega \tag{A.3}$$

where the dispersivity tensor Λ_f corresponds to a dispersion restricted to the fluid phase, assuming impervious boundary conditions at the fluid–solid interface. Two source terms are present in this equations: s is a volumetric heat source present in the fluid phase while $\boldsymbol{q}_{s\to f}$ corresponds to the heat flux exchanged at the solid/fluid interface $\partial\Omega_{sf}$, that is the flux that stems from the solid temperature gradient at the solid/fluid interface in the sphere of volume V:

$$Vq_{s\to f}=-\int_{\partial V_{sf}}\lambda_s\nabla T_s\cdot\boldsymbol{n}_{sf}\mathrm{d}S. \tag{A.4}$$

It is possible to write the heat diffusion equation for this local temperature in the solid phase

$$(\rho c_p)_s\frac{\partial T_s}{\partial t}=\nabla\cdot(\lambda_s\nabla T_s)\quad\text{in }V_s. \tag{A.5}$$

Application of the solid phase averaging operator (A.1) to this equation yields the heat balance equation for the solid phase intrinsic temperature

$$\begin{aligned}(\rho c_p)_s\frac{\partial\langle T_s\rangle^s}{\partial t}&=\frac{1}{V_s}\int_{V_s}\nabla\cdot(\lambda_s\nabla T_s)\mathrm{d}V\\&=\frac{1}{V_s}\int_{\partial V_{sf}}\lambda_s\nabla T_s\cdot\boldsymbol{n}_{sf}\mathrm{d}S\\&=-\frac{1}{(1-\varepsilon)}q_{s\to f}\quad\text{in }\Omega.\end{aligned} \tag{A.6}$$

The boundary condition of Eq. (A.5) is given here by an imposed fluid temperature $T_s=T_f$ at the boundary ∂V_{sf} of the solid particles present in the sphere.

We assume here that, at the local scale, the fluid temperature T_f is uniform in the fluid part V_f of volume V and that, at initial time, the whole temperature field in Ω is uniform at a reference temperature T_{ref}, with $T_{ref}=0$, see Eq. (7f). With these conditions, Eq. (A.5) can be written in the Laplace domain:

$$\nabla\cdot(\lambda_s\nabla\widetilde{T}_s)=(\rho c_p)_s p\widetilde{T}_s\quad\text{in}\quad V_s\quad\text{with}\quad\widetilde{T}_s=\widetilde{T}_f\quad\text{in }\partial V_{sf} \tag{A.7}$$

Since system (A.7) is linear with a unique excitation $T_f(t)$, its solution is a convolution product in time and a simple product in the Laplace domain, and the solid phase averaging operator (A.1) can be used:

$$\widetilde{T}_s(P)=\tilde{e}(P)\widetilde{T}_f\Rightarrow\langle\widetilde{T}_s\rangle^s-\widetilde{T}_f=(\langle\tilde{e}\rangle^s-1)\widetilde{T}_f, \tag{A.8}$$

where e is the Green's function of the problem that depends both on point P and on time t. The Laplace transform can be applied to Eq. (A.4), and substitution of the Laplace transform (A.8) of the fluid temperature yields:

$$\tilde{q}_{s\to f}=a_{sf}p\tilde{h}(\langle\widetilde{T}_s\rangle^s-\widetilde{T}_f) \tag{A.9}$$

where $a_{sf}=\frac{|\partial V_{sf}|}{V}$ is the specific area, and $p\tilde{h}=\frac{1}{(1-\langle\tilde{e}\rangle^s)}\frac{1}{|\partial V_{sf}|}\int_{\partial V_{sf}}\lambda_s p\nabla\tilde{e}\cdot\boldsymbol{n}_{sf}\mathrm{d}S$.

A usual approximation, that will be valid for the large time values, is given by: $h_\infty=\lim_{p\to0}(p\tilde{h})$.

The heat exchange between the two phases, per unit volume of porous medium, can be expressed using a convolution product, noted here by a star, in the time domain, that is,

$$q_{s\to f}=a_{sf}h*\frac{\partial}{\partial t}(\langle T_s\rangle^s-T_f)\approx a_{sf}h_\infty(\langle T_s\rangle^s-T_f). \tag{A.10}$$

The 'volumetric' heat exchange impedance h or the h_∞ coefficient can be calculated in the case of spherical grains. For a uniform temperature $T_f(t)$ of the fluid at the local scale, and a zero uniform initial temperature for the whole system, the intrinsic average solid temperature $\langle T_s\rangle^s$ is in fact the average temperature of the local internal temperature field in the volume V_{sphere} of the grain, that is one-dimensional in the radial (r) direction. This means that one can take $V_s=V_{sphere}$ for this averaging

$$\langle T_s\rangle^s(t)=\frac{1}{V_{sphere}}\int_0^R T_s(r,t)(4\pi r^2)\mathrm{d}r\quad\text{with}\quad V_{sphere}=\frac{4}{3}\pi R^3. \tag{A.11}$$

The solution of (A.7), with $\nabla^2=\partial^2/\partial r^2+(2/r)\partial/\partial r$, is: $\widetilde{T}_s=\frac{R}{r}\frac{\sinh(kr)}{\sinh(kR)}\widetilde{T}_f=\tilde{e}\widetilde{T}_f$ with $k^2=p/a$.

The Laplace transform of the Green's function e allows the calculation of the volumetric impedance $p\tilde{h}$:

$$p\tilde{h}=\frac{\lambda_s}{R}\frac{q^2(q\coth q-1)}{3(q\coth q-1)-q^2}\quad\text{with}\quad q=R\sqrt{p/a_s}. \tag{A.12}$$

An asymptotic series expansion can be found for low values of p and consequently, of q. This development is valid for large times, that is under quasi (local) steady state conditions:

$$q\coth q=1+\frac{1}{3}q^2+\frac{1}{45}q^4+\mathrm{O}(q^6)\Rightarrow p\tilde{h}=\frac{5\lambda_s}{R}(1+\mathrm{O}(q^2)). \tag{A.13}$$

This gives the value of the asymptotic 'volumetric' heat exchange coefficient $h_\infty=10\lambda_s/d$ while the specific surface is $a_{sf}=6(1-\varepsilon)/d$ for a granular bed of solid spheres. The two coupled Eqs. (A.3) and (A.6) of the Coats–Smith two-temperature model can be solved in a two dimensional case for a uniform filtration velocity $u=u_{Dx}$ and for the following form of the interface heat flux and of the source term:

$$q_{s\to f}=a_{sf}h_\infty(\langle T_s\rangle^s-\langle T_f\rangle^f)\quad\text{and}\quad s=Q\delta(x)\delta(y)H(t). \tag{A.14}$$

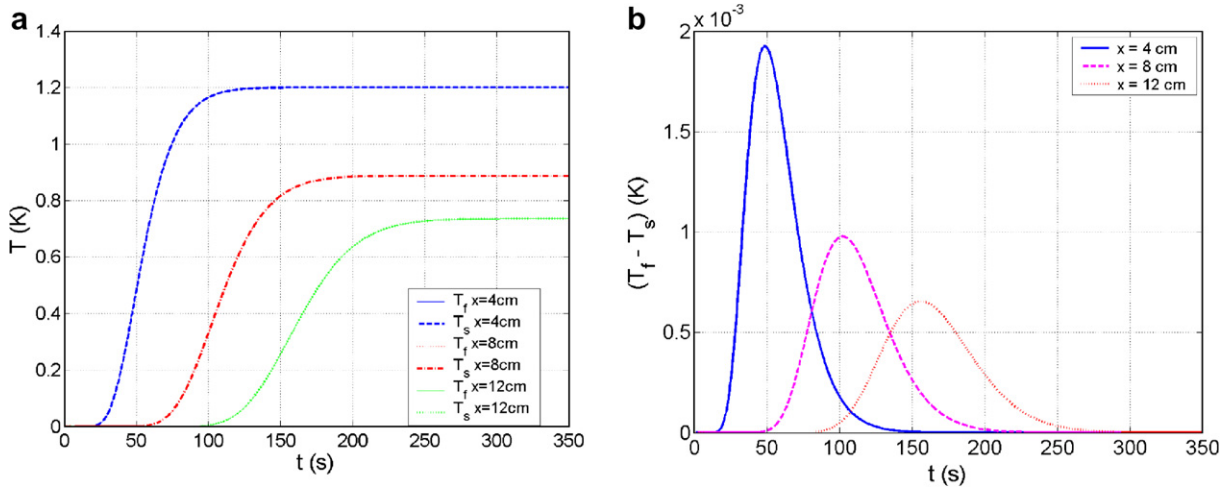

Fig. A. Simulated thermograms – Coats–Smith model. (a) Temperatures of fluid and solid phase and average enthalpic temperature ($y = 0$) for $Pe = 35$, $Q = 10\ \mathrm{J\ m^{-2}}$; $\lambda_x = 1.15\ \mathrm{W\ m^{-1}\ K^{-1}}$; $\lambda_y = 0.267\ \mathrm{W\ m^{-1}\ K^{-1}}$. (b) Difference between the temperatures of the fluid and solid phases.

The solution, in the Laplace domain, is:

$$\langle \widetilde{T}_\mathrm{f} \rangle^\mathrm{f} = \frac{Q}{2\pi\sqrt{\Lambda_{\mathrm{f}x}\Lambda_{\mathrm{f}y}}} \frac{1}{p} \exp\left(\frac{(\rho c_p)_\mathrm{f} u x}{2\Lambda_{\mathrm{f}x}}\right) \times K_0\left(\left(\frac{x^2}{\Lambda_{\mathrm{f}x}} + \frac{y^2}{\Lambda_{\mathrm{f}y}}\right)^{1/2} \sqrt{\ell^2 + \frac{(\rho c_p)_\mathrm{f}^2 u^2}{4\Lambda_{\mathrm{f}x}}}\right) \quad \text{(A.15)}$$

$$\langle \widetilde{T}_\mathrm{s} \rangle^\mathrm{s} = \frac{a_\mathrm{sf} h_\infty}{(1-\varepsilon)(\rho c_p)_\mathrm{s} p + a_\mathrm{sf} h_\infty} \langle \widetilde{T}_\mathrm{f} \rangle^\mathrm{f} \quad \text{(A.16)}$$

with

$$l^2 = p\left[\varepsilon(\rho c_p)_\mathrm{f} + (1-\varepsilon)(\rho c_p)_\mathrm{s} \frac{a_\mathrm{sf} h_\infty}{(1-\varepsilon)(\rho c_p)_\mathrm{s} p + a_\mathrm{sf} h_\infty}\right].$$

Numerical Laplace inversion of Eqs. (A.15) and (A.16), see [22], making the coefficients of the dispersitivity tensor Λ_f equal to the dispersion coefficients λ_x and λ_y of the one-temperature model, allows the calculation of the solid and fluid temperature responses $\langle \widetilde{T}_\mathrm{s} \rangle^\mathrm{s}$ and $\langle \widetilde{T}_\mathrm{f} \rangle^\mathrm{f}$ and, consequently to the reconstruction of the average temperature T_H according to (A.2).

The three temperature curves have been plotted in Fig. A(a), for the air/glass beads system, for different downstream locations x (for $y = 0$), see Fig. 1. The Péclet number is equal to 35 here and the corresponding values of the dispersion coefficients stem from the experimental correlations (29) and (30). The three curves overlap and cannot be separated: the fluid, solid and average temperature responses are equal in practice. The temperature difference between fluid and solid is magnified in Fig. A(b). For a total temperature increase close to 1 K, the maximum difference is equal to 2×10^{-3} K for $x = 4$ cm. This maximum temperature difference occurs at the half rise time (50 s approximately for $x = 4$ cm, 110 s for $x = 8$ cm and 170 s for $x = 12$ cm) and this difference decreases later on to vanish completely for steady state conditions. The average temperature curve T_H, nearly equal to the solid temperature here, corresponds also to the output of the one temperature model (6).

Other simulations have shown that the thermal desequilibrium between fluid and solid increases with lower values of the solid phase conductivity. A solid conductivity equal to the conductivity of air ($\lambda_\mathrm{s} = 0.026\ \mathrm{W\ m^{-1}\ K^{-1}}$) yields maximum temperature differences of the order of 0.1 K for a maximum temperature rise close to 1.3 K (for $x = 4$ cm). This very low level of solid conductivity can only be met for aerogel grains where Knudsen effect (rarefied gases) takes place because of the nanometric scale of the pores. One can conclude that, for common levels of the solid conductivity, thermal desequilibrium does not appear, even under transient conditions. This conclusion is only valid if no heat source – a chemical reaction for example – is present in the solid or fluid phase close to the locations where these temperatures are observed.

References

[1] S. Yagi, D. Kunii, N. Wakao, Studies on axial effective thermal conductivities in packed beds, AIChE J. 6 (1960) 543–546.
[2] J. Vortruba, V. Hlavacek, M. Marek, Packed bed axial thermal conductivity, Chem. Eng. Sci. 27 (1972) 1845–1851.
[3] A.G. Dixon, D.L. Cresswell, Theoretical prediction of effective heat transfer parameters in packed beds, AIChE J. 25 (1979) 663–676.
[4] D.J. Gunn, J.F.C. De Souza, Heat transfer and axial dispersion in packed beds, Chem. Eng. Sci. 29 (1974) 1363–1371.
[5] E. Tsotas, Über die Wärme- und Stoffübertragung in durchströmten Festbetten, Fortschrittberichte, Reihe 3, Nr. 223, VDI, Düsseldorf, 1990.
[6] R. Bauer, E.-U. Schlünder, Effective radial thermal conductivity of packings in gas flow. Part I: Convective transport coefficient, Int. Chem. Eng. 18 (1978) 181–188.
[7] J. Levec, R.G. Carbonell, Longitudinal and lateral thermal dispersion in packed beds, AIChE J. 31 (1985) 581–601.
[8] F. Zanotti, R.G. Carbonell, Development of transport equations for multiphase systems, III, Chem. Eng. Sci. 39 (1984) 299–311.
[9] H. Martin, Low Péclet number particle-to-fluid heat and mass transfer in packed beds, Chem. Eng. Sci. 33 (1978) 913–919.
[10] T. Metzger, S. Didierjean, D. Maillet, Optimal experimental estimation of thermal coefficients in porous media, Int. J. Heat Mass Transfer 47 (2004) 3341–3353.

[11] C. Moyne, S. Didierjean, H.P. Amaral Souto, O.T. Da Silveira, Thermal dispersion in porous media: One-equation model, Int. J. Heat Mass Transfer 43 (2000) 3853–3867.
[12] M. Fourar, G. Radilla, R. Lenormand, C. Moyne, On the non-linear behavior of a laminar single-phase flow through two and three-dimensional porous media, Adv. Water Resour. 27 (2004) 669–677.
[13] G. Schneebeli, Expériences sur la limite de validité de la loi de Darcy et l'apparition de la turbulence dans un écoulement de filtration, La Houille Blanche 10 (1955) 141–149.
[14] A.E. Scheidegger, The physics of flow through porous media, University of Toronto Press, 1960.
[15] P. Forcheimer, Wasserberwegung durch Boden, Z. Vereines deutscher Ing 45 (1901) 1782–1788.
[16] N. Ozisik, Heat Conduction, second ed., Wiley, Chichester, 1980.
[17] K. H Coats, B.D. Smith, Dead end pore volume and dispersion in porous media, Soc. Petroleum Eng. J. 4 (1964) 73–84.
[18] J.V. Beck, K.J. Arnold, Parameter estimation in engineering and science, Wiley, Chichester, 1977.
[19] T. Metzger, Dispersion thermique en milieux poreux: caracactérisation expérimentale par technoque inverse (Thermal dispersion in porous media: Experimental characterization by an inverse technique), Ph.D. thesis, INPL Nancy, France, October 28, 2002.
[20] A. Testu, Dispersion thermique dans les milieux granulaires: caractérisation à coeur et en proche paroi (Thermal dispersion in granular media: core and near wall characterization), Ph.D. thesis, INPL Nancy, France, November 23, 2005.
[21] M. Quintard, M. Kaviany, S. Whitaker, Two-medium treatment of heat transfer in porous media: Numerical results for effective properties, Adv. Water Resour. 20 (1997) 77–94.
[22] D. Maillet, S. André, J.C. Batsale, A. Degiovanni, C. Moyne, Thermal Quadrupoles – Solving the Heat Equation through Integral transforms, Wiley, Chichester, 2000.